Inorganica Chimica Acta 499 (2020) 119198

Contents lists available at ScienceDirect

Inorganica Chimica Acta

journal homepage: www.elsevier.com/locate/ica

Research paper

$[NH_4]_{12}[(MoO_2)_2O(HPO_4)_2]_4[PO_4]Cl{\cdot}0.5H_2O$: A mixed phosphomolybdate with nonlinear optical properties

Zhongqi Jiang[a], Wenqiang Chen[a], Qun Jing[a], Ming-Hsien Lee[b], Zhaohui Chen[a,*]

[a] College of Chemistry and Chemical Engineering & College of Physical Science and Technology, Xinjiang University, 666 Shengli Road, Urumqi 830046, China
[b] Department of Physics, Tamkang University, New Taipei City 25137, Taiwan

ARTICLE INFO

Keywords:
Phosphomolybdates
Nonlinear optical properties
Theory calculations
Noncentrosymmetric

ABSTRACT

Phosphates usually have shorter ultraviolet (UV) absorption edges and are ideal for deep-UV nonlinear optical (NLO) applications. The introduction of d^0 transition metal cation Mo^{6+} into phosphates can facilitate to increase the distortion of the crystal structure and therefore it is easy to obtain the noncentrosymmetric (NCS) compounds, which are expected for NLO materials. In the work, the crystals of an ammonium molybdenophosphate chloride $[NH_4]_{12}[(Mo_2)_2O(HPO_4)_2]_4[PO_4]Cl{\cdot}0.5H_2O$ (AMPC) were grown by hydrothermal method. The second harmonic generation (SHG) of the compound exhibits 0.3 × KH_2PO_4 (KDP) at 1064 nm radiation and the cutoff edge of it is about 230 nm. The crystal structure is consist of unique $[Mo_4P_4O_{32}H_4]^{16-}$ units and further to form layer two-dimensional (2D) structure. The first-principles electronic structure calculations show that the NLO response of it mainly comes from the Mo-O units. We also studied UV–*vis*-NIR diffuse reflectance, infrared spectrum and thermal properties of the compound. Additional, by the investigation of similar phosphomolybdates, we found that they have high ratios of NCS crystal structures about 39%.

1. Introduction

Nowadays, it is a very important way to increase solid-state laser sources by nonlinear optical (NLO) crystals frequency conversion, which can be used in atmospheric monitoring, laser medical treatment, laser radar and fundamental research [1–6]. Borates have always been hotspots due to their rich structural chemistry and intrinsic properties, such as LiB_3O_5 (LBO) [7], β-$Ba_2B_2O_4$ (β-BBO) [8] and $KBe_2BO_3F_2$ (KBBF) [9] practically available benchmark NLO materials, α-BaB_2O_4 [10] and $Ca(BO_2)_2$ [11] as birefringent materials. But as deep ultraviolet (DUV) (< 200 nm) NLO materials, they all have their own defects. For example, LBO, with a short absorption edge (155 nm), but small birefringence making phase matching difficult; β-BBO, with strong second harmonic generation (SHG), but suffering from large birefringence and walk-off effect; KBBF, the only one applicable in DUV but with insurmountable layered growth nature and highly toxic beryllium component [12–14]. Therefore, the identification of new UV and DUV NLO materials is still of great urgent demand. Scientists have proposed different ideas on how to design noncentrosymmetric (NCS) materials with large SHG and short cutoff edge NLO materials [15–19]. Fluorooxoborates, new prolific fields for exploring UV and DUV materials, are potential for designing structure types favorable to excellent optical properties developed by Pan group recent years [20–25].

Phosphates, which are newly attractive candidates for DUV NLO materials, have gained extensive attentions because of abundant P—O groups and short cutoff edges. Furthermore, SHG responses in orthophosphates can be enhanced by highly polymerized P—O groups, nonbonded O-2p orbitals in PO_4 tetrahedron [26,27]. In recent years, we have explored some phosphates with novel crystal structures and good performance [28–31]. In order to make it easier to obtain NCS compounds and enrich the structural chemistry of phosphates, d^0 transition metal cations can be introduced to increase distortion and polarization [32]. It is well known that the sequence of cations distortion of d^0 transition metals is $Mo^{6+} > V^{5+} > W^{6+} > Nb^{5+} > Ta^{5+} > Ti^{4+}$ [33], in which Mo^{6+} is susceptible to second-order Jahn-Teller (SOJT) distortions and is conducive to design materials with better SHG efficiency [34]. Therefore, the combination of the Mo-O and P—O groups may be feasible strategy to design NCS materials with good optical properties. So far, only a few molybdenophosphates have been reported as NLO materials, such as $Rb_4Mo_5P_2O_{22}$ [35], $Cs_4Mo_5P_2O_{22}$ [4]. By the investigation of ammonium phosphomolybdates we found that the proportion of them with NCS structure is up to 39%, which far higher than other types of compounds (Table S1) [36–45]. In this work, the crystal of $[NH_4]_{12}[(MoO_2)_2O(HPO_4)_2]_4[PO_4]Cl{\cdot}0.5H_2O$ (AMPC) compound was synthesized and combines semi-molecular water compared to $[NH_4]_{12}[(MoO_2)_2O(HPO_4)_2]_4[PO_4]Cl$ crystal reported by Weller et al

* Corresponding author.
E-mail address: chenzhaohui686@sina.cn (Z. Chen).

https://doi.org/10.1016/j.ica.2019.119198
Received 17 September 2019; Received in revised form 5 October 2019; Accepted 5 October 2019
Available online 08 October 2019

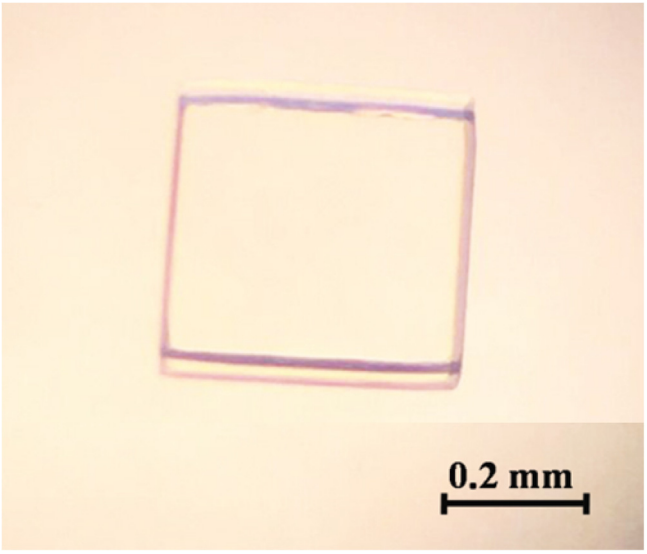

Fig. 1. Photograph of the AMPC crystal.

in 2009 [46]. It exhibits a moderate SHG response approximate 0.3 × KDP. Furthermore, diffuse reflectance spectrum shows its cutoff edge is about 230 nm and down to UV spectral region. In this work, we report on the crystal growth and optical properties of the AMPC compound. In addition, thermal behavior, electronic band structure calculations of the title compound were also presented.

2. Experimental section

2.1. Crystal growth

Crystals of AMPC were prepared via hydrothermal method. The mixture of 0.2420 g (1.0 mmol) $Na_2MoO_4{\cdot}2H_2O$, 0.690 g (6.0 mmol) $NH_4H_2PO_4$, 0.2674 g (5.0 mmol) NH_4Cl, 0.1237 g (2.0 mmol) H_3BO_3 and 1 ml deionized water were put into a 23 ml polytetrafluoroethylene lining, respectively, then sealed it and shifted into a steel coat. They were put into a resistance furnace and heated to 210 °C gradually, held for 24 h, and then reduced to 150 °C at a rate of 1 °C/h, finally to room temperature at a rate of 5 °C/h. Here, H_3BO_3 was used as the mineralizing agent in the reaction. After that, the Teflon liner was opened in air and colorless and transparent crystals were obtained (Fig. 1) in a yield of *ca* 71% based on molybdenum element.

2.2. Single-Crystal structure determination

A transparent crystal (0.20 × 0.15 × 0.12 mm^3) was used for single crystal X-ray determination collection. The diffraction data were collected on a Bruker Smart APEX II charge-coupled device (CCD) single crystal diffractometer (graphite monochromatic Mo-K_α radiation, λ = 0.71073 Å) at room temperature and integrated with the SAINT program. The numerical absorption corrections were performed with the SADABS program [47]. The structure was solved by direct methods and refined by the full-matrix least-squares method with anisotropic displacement parameters in SHELXL-97 system [48]. It was checked with aid of the program PLATON [49]. Crystal parameters, data collections, and structure refinement information are given detailed in Table 1. Atoms coordinates with isotropic and equivalent displacement parameters are summarized in Tables S2 and S3 in the Supporting Information.

2.3. Powder X-ray diffraction

The selected transparent tetragonal crystals were dried naturally, ground into a uniform powder by agate grinding. The powder XRD measurement was carried out using a Bruker D8 PHASER X-ray diffractometer equipped with Cu Ka radiation (l = 1.5418 Å) at room temperature. The 2θ range was 5–70°with a scan step width of 0.02 and a fixed counting time of 1s per step. The powder XRD curve is consistent with that one simulated from single-crystal structure in Fig. S1.

Table 1
Crystal data and structure refinement for AMPC.

Empirical formula	$[NH_4]_{12}[(MoO_2)_2O(HPO_4)_2]_4[PO_4]Cl{\cdot}0.5H_2O$
Formula weight	2211.27
Temperature [K]	150(2)
Wavelength [Å]	0.71073
Crystal system	Tetragonal
Space group	P_4_4
Unit cell dimensions	a = 9.7089(4) Å b = 9.7089(4) Å c = 14.5943(16) Å
Volume [$Å^3$]	1375.70(19)
Z	1
Calculated density [Mg/m^3]	2.669
Absorption coefficient [mm^{-1}]	2.215
F(0 0 0)	1081
Crystal size [mm^3]	0.19 × 0.15 × 0.08
Theta range for data collection [°]	2.967 to 27.523
Limiting indices	$-12 \le h \le 12$, $-12 \le k \le 12$, $-18 \le l \le 16$
Reflections collected/unique	18,724/3157 [R(int) = 0.0217]
Completeness to theta = 25.242[%]	99.5
Refinement method	Full-matrix least-squares on F_o^2
Data/restraints/parameters	3157/25/244
Goodness-of-fit on F_o^2	1.116
Final R indices [I > 2sigma(I)]$^\alpha$	R_1 = 0.0139, wR_2 = 0.0341
R indices (all data)$^\alpha$	R_1 = 0.0142, wR_2 = 0.0342
Extinction coefficient	0.0030(2)
Largest diff. peak and hole [$e{\cdot}Å^{-3}$]	0.602 and −0.550

$^aR_1 = \Sigma||F_o| - |F_c||/\Sigma|F_o|$ and $wR_2 = [\Sigma w(F_o^2 - F_c^2)^2/\Sigma wF_o^4]^{1/2}$ for $F_o^2 > 2\sigma(F_o^2)$.

2.4. Thermal analysis

Thermal gravimetric (TG) and Differential Thermal Analysis (DTA) analyses were carried out on a HITACHI STA 7300 thermal analyzer instrument at a temperature range of 30–500 °C with a heating rate of 10 °C·min^{-1} and then cooled to room temperature at the same rate under flowing argon.

2.5. Spectroscopy analysis

UV–*vis*-NIR diffuse-reflectance data were collected with a SolidSpec-3700DUV spectrophotometer using polytetrafluoroethylene as a standard in the wavelength range from 190 to 2600 nm. Absorption (K/S) data were calculated from the following Kubelka-Munk function: $F(R) = (1 - R)^2/2R = K/S$; where R is the reflectance, K is the absorption, and S is the scattering [50,51].

The IR spectrum was measured with a Shimadzu IRAffinity-1 Fourier transform IR spectrometer in the 400–4000 cm^{-1} range, the sample was mixed thoroughly with dried KBr.

2.6. Energy spectrum analysis

In order to further verify the elements contained in AMPC compound, Hitachi's new high resolution field emission scanning electron microscope SU8010 was used for EDS test of the compound. It can be seen from Fig. S2 that the crystal contains the five elements N, Mo, P, O and Cl. The results are consistent with crystal structure analysis.

2.7. Second-Order NLO measurements

The SHG intensities of AMPC crystals were evaluated using the Kurtz Perry method [52]. The measurements were carried out using a Nd:YAG pulsed solid-state laser (1064 nm, 10 kHz, 10 ns) [53]. The output light intensity emitted from the samples was collected using a photomultiplier tube. For the reason that the SHG efficiency depends strongly on particle sizes [54], polycrystalline AMPC samples were ground and sieved into the following particle size ranges: 0–20, 20–38, 38–55, 55–88, 88–105, 105–150, 150–200 mm. The microcrystalline KDP samples with the same particle size ranges were served as the references.

2.8. Computational descriptions

First-principles density functional theory (DFT) electronic structure calculations for the compound were performed with the CASTEP code [55]. During the calculation, the generalized gradient approximation (GGA) with Perdew-Burke-Ernzerhof (PBE) functional was adopted [56]. The interactions between the ionic cores and the electrons were described by the ultrasoft pseudopotentials [57,58], the following orbital electrons were treated as valence electrons: Mo, $4d^5 5s^1$; P, $3s^2 3p^3$; O, $s^2 2p^4$; Cl, $3s^2 3p^5$; N, $2s^2 2p^3$; H, $1s^1$. The kinetic energy cutoff of 830 eV was chosen, and the numerical integration of the Brillouin zone was performed using a 3 × 3 × 2 Monkhorst-Pack *k*-point sampling. The other calculation parameters and convergent criteria were the default values of the CASTEP code [59,60].

3. Results and discussion

3.1. Crystal structure description

AMPC crystallizes in the tetragonal system with space group of *P*_4_4. In the asymmetric units, there are two unique molybdenum atoms, three unique phosphorus atoms, sixteen unique oxygen atoms, one unique chlorine atom, four unique nitrogen atoms and fifteen hydrogen atoms, as shown in Table S4 and Fig. 2. Three P atoms coordinate with four O atoms to form PO_4 tetrahedra, P(1) and P(2) are connected to hydrogen to form PO_4H groups. All Mo atoms coordinate with six O atoms to form MoO_6 polyhedra. As shown in Fig. 3(a), in the crystal structure, there are two unique $[Mo_4P_4O_{32}H_4]^{16-}$ units, which can be clearly seen along the *b*-axis direction as an eight-membered ring (Fig. 3(b)) composed of MoO_6 polyhedra and HPO_4 groups, which by sharing vertex O atoms along the *c*-axis and further form a network structure in Fig. 3(c). As shown in Fig. 3(d), the crystal structure is similar to the cell membrane structure viewed along *b*-axis. The layer formed by the $_\infty[Mo_4P_4O_{28}H_4]^{8-}$ units is similar to the phospholipid molecular layer in the cell membrane. NH_4^+ ions, Cl^- ions and isolated PO_4^{3-} groups are filled between the layers, which are further interconnected by hydrogen bonds (see Fig. 3(d)). By comparing the atomic numbers on both sides of the *b*-axis, it is found that there is a high degree of symmetry in the crystal structure.

There are three kinds of hydrogen bonds in the crystal, namely N—H…Cl, N—H…O and O—H…O. As shown in Fig. 4(a), the Cl^- anions are at the center, and the remaining six NH_4^+ ions are dispersed on the surface of the sphere at a certain radius from the Cl^- ion and the hydrogen bond lengths range from 2.556 to 3.243 Å. As shown in Fig. 4(b), the H_2O molecule generates hydrogen bonds with four NH_4^+ cations with hydrogen bond distances ranging from 2.401 to 3.243 Å. In Fig. 4(c), the isolated PO_4^{3-} group forms hydrogen bonds with OH^- (PO_4H group) and NH_4^+ ions, wherein the hydrogen bond distances are range from 1.640 to 1.736 Å, the isolated hydrogen bond distance between the PO_4^{3-} group and the NH_4^+ ion ranges from 2.682 to 3.514 Å. It can be seen that AMPC compound has complex hydrogen bonds networks.

3.2. Thermal analysis

As can be seen from Fig. 5, the TG curve shows that AMPC crystal is stable before 160 °C, then continuous weight loss occurs between 160 and 500 °C. The overall weight loss was about 30.1% at the temperature range. Through theoretical calculation of the corresponding

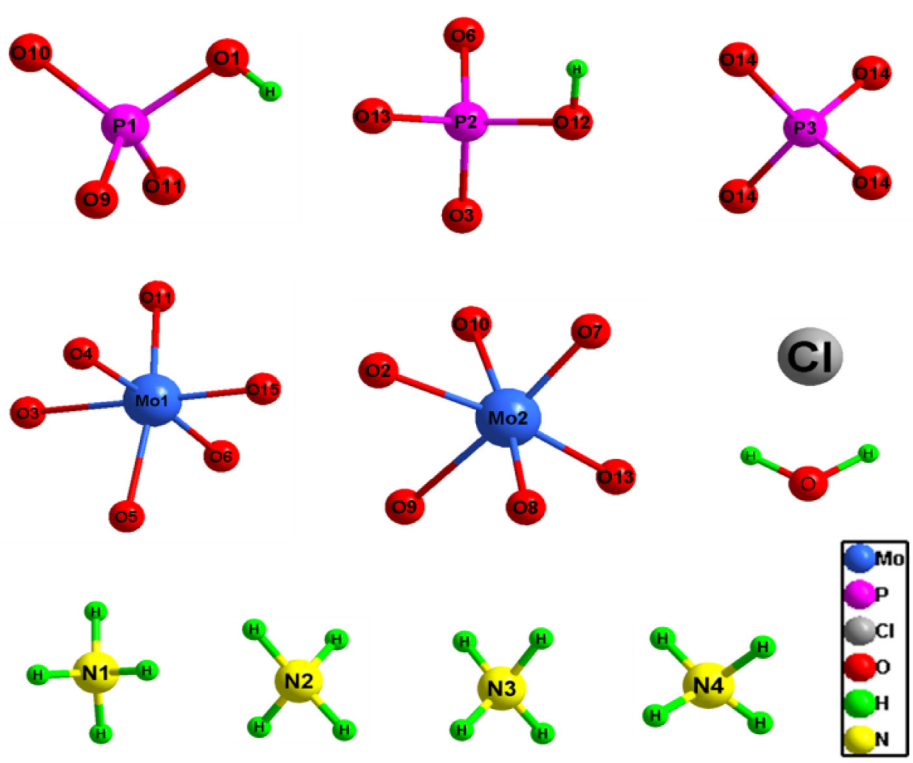

Fig. 2. Coordination environment in AMPC.

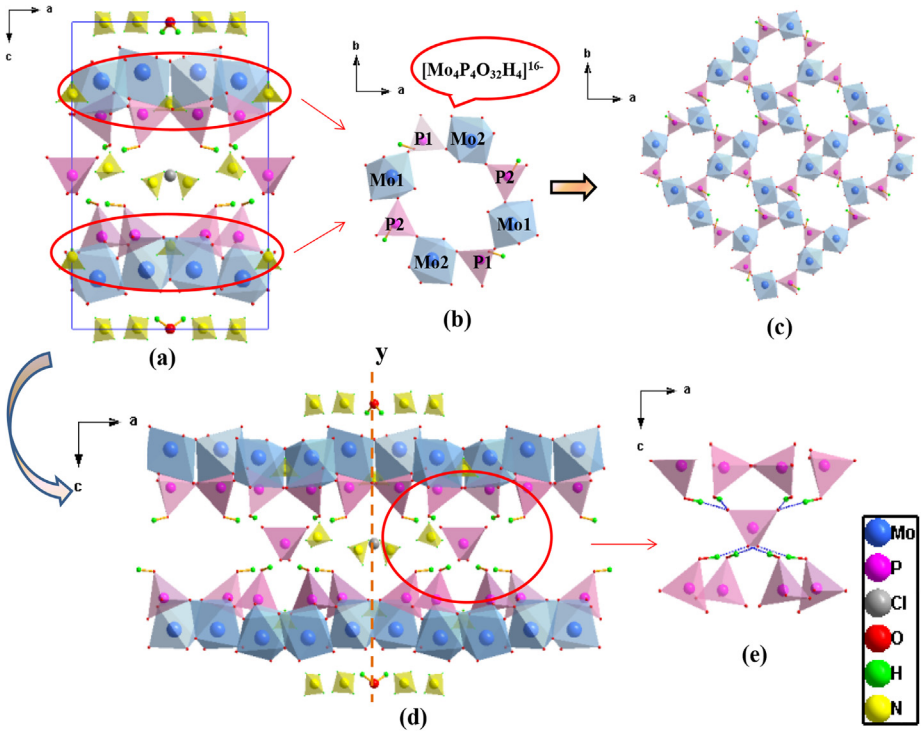

Fig. 3. The structure of AMPC: (a) Unit cell structure viewed along *b* axis, (b) $[Mo_4P_4O_{32}H_4]^{16-}$ eight-membered ring, (c) $_\infty[Mo_4P_4O_{32}H_4]^{16-}$ shapes a network structure viewed along *c* axis, (d) The whole of a polyhedron. (The MoO_6 polyhedra are show in blue; the PO_4 tetrahedra are show in pink); (e) The layers are connected by hydrogen bonds. (For interpretation of the references to colour in this figure legend, the reader is referred to the web version of this article.)

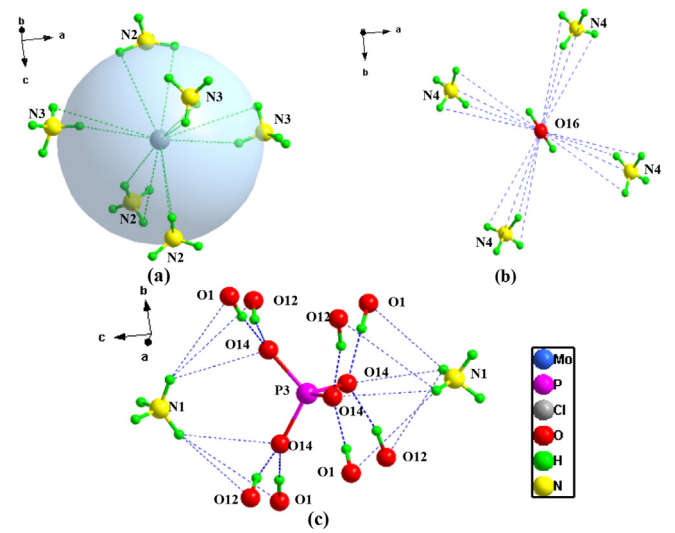

Fig. 4. The hydrogen bonds of AMPC: (a) Hydrogen bonds between Cl^- and NH_4^+ (b) Hydrogen bonds between H_2O molecule and NH_4^+ (c) Hydrogen bonds between isolated PO_4^{3-} and OH^-, NH_4^+.

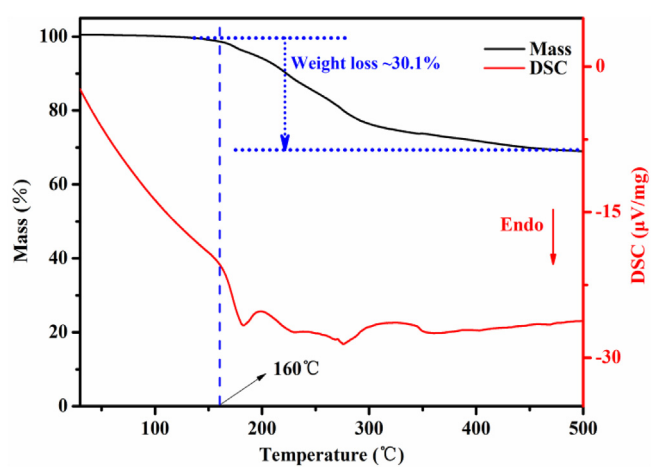

Fig. 5. TG-DSC curves of AMPC crystals.

decomposable groups, hydrogen chloride and ammonia account for about 28.3%, which are roughly consistent with the weight loss values. In the DTA curve, there are multiple endothermic peaks in the range from 160 to 350 °C, indicating that AMPC crystal has multistep decomposition reaction.

3.3. Spectral analysis

As can be seen from the reflectance spectrum in Fig. 6, no obvious absorption peak was observed in the range of 450–2600 nm and the cutoff edge is below 230 nm and the optical band gap of AMPC is about 3.11 eV.

IR spectroscopic measurement is shown in Fig. S1. The absorption bands around 3263 cm^{-1} are the stretching vibration of N—H in NH_4^+ and O—H in water. The infrared absorption peaks at 1446 and 1412 cm^{-1} are due to the vibration of N—H. The absorption peaks at 1287 and 1095 cm^{-1} are asymmetric stretching vibration of P—O in the PO_4 units, and the absorption peaks at 732 and 550 cm^{-1} may be symmetric stretching and bending vibration of P—O in the PO_4 units respectively. The absorption peak at 880 cm^{-1} is the stretching vibration of Mo-O in the MoO_6 polyhedra.

3.4. Second-Order NLO measurements

Owing to NCS compound, it is worth studying SHG properties of the compound. Powder SHG measurements using 1064 nm radiation revealed that the SHG efficiency of it is approximately 0.3 × KDP as shown in Fig. 7. As mentioned above, the weaker SHG efficiency may be due to the material's nonpolar space group that does not have a constructive addition of net moments.

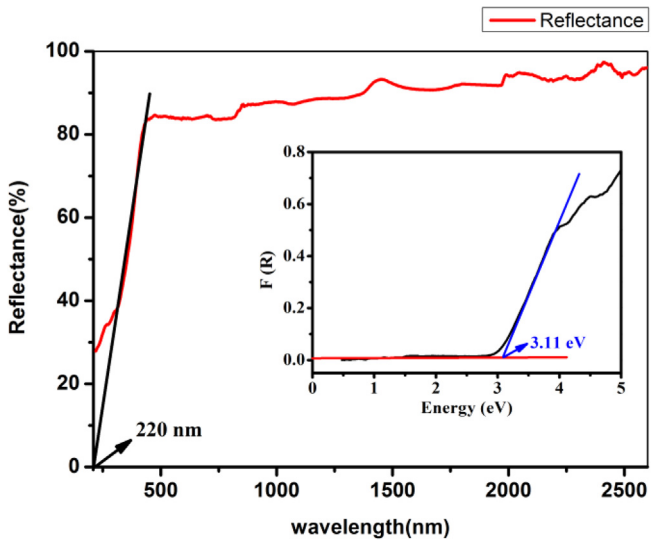

Fig. 6. The UV–*vis*-IR diffuse reflectance spectrum of AMPC.

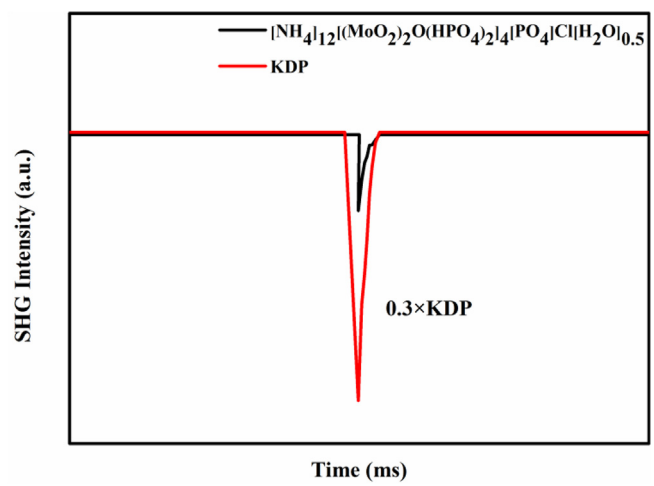

Fig. 7. The SHG of AMPC.

3.5. Electronic structure

Consequently, in order to better understand the intrinsic relationship between the crystal structure and optical properties, electronic structure calculations of AMPC were performed. As shown in Fig. 8, the compound is a direct band gap compound with band gap value of 1.05 eV, which is smaller than experimental optical gap, which attributes to the discontinuity of the PBE functional in DFT calculations. The covalent interaction between Mo and O states results in shorter Mo and O bonds in AMPC and lower energy transfer in O-2p state also leads to the reduction of band gap.

In order to investigate the origination of SHG, we studied the electronic and optical properties of AMPC using the first-principle DFT method. From the PDOS of AMPC (Fig. 9), it can be seen that the energy window near the Fermi energy level is mainly composed of Mo-d, O-p and P-p orbitals. However, the top of the valence band is almost entirely composed of O-p orbitals, while the bottom of the conduction band is mainly composed of Mo-d orbitals and the contributions of P-p, Cl-p, *N*-p and H-s orbitals are relatively small. Therefore, the electronic structure around Fermi energy level comes from the Mo-O groups, which determines the optical properties of the compound.

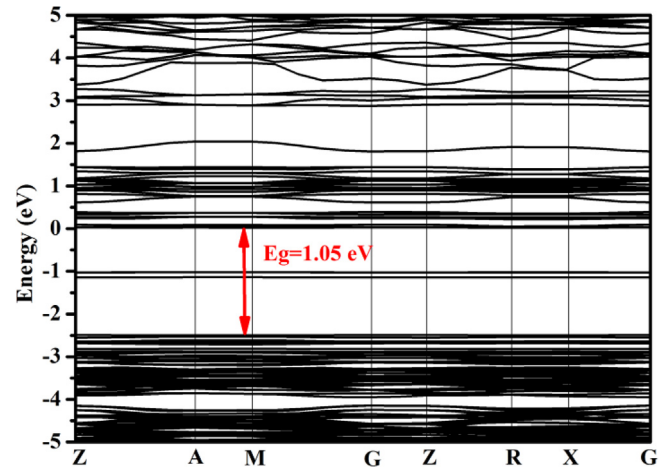

Fig. 8. The electronic band structure of AMPC.

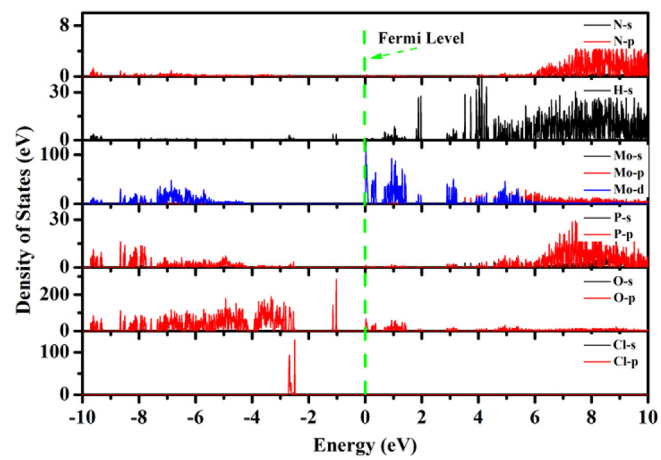

Fig. 9. The projected density of states (PDOS) of AMPC.

4. Conclusion

In summary, the crystals of AMPC were synthesized by hydrothermal method. Bilayers of phospholipid in the cell membrane structure are formed by unique $[Mo_4P_4O_{32}H_4]^{8-}$ repeat units. The SHG effect of the compound is 0.3 times that of KDP and the cutoff edge is below 230 nm. The study shows that the possibility of NCS structures can be greatly improved by introducing Mo ions, which are favorable for exploring new NLO optical materials. Theoretical calculations show that optical effect is mainly derived from Mo-O groups. In addition, thermal properties, elements analysis and infrared spectroscopy are also presented. The research opens a new window for the search and design new ammonium molybdenophosphates NLO materials.

Accession codes

CCDC 1943837 contains the supplementary crystallographic data for this paper. These data can be obtained free of charge via www.ccdc.cam.ac.uk/data_request/cif, or by emailing data_request@ccdc.cam.ac.uk, or by contacting The Cambridge Crystallographic Data Centre, 12 Union Road, Cambridge CB2 1EZ, UK; fax: + 44 1223 336033.

Acknowledgements

This work is supported by the Natural Science Foundation of Xinjiang Uygur Autonomous Region of China (Grant 2018D01C045).

Appendix A. Supplementary data

Supplementary data to this article can be found online at https://doi.org/10.1016/j.ica.2019.119198.

References

[1] P.S. Halasyamani, K.R. Poeppelmeier, Noncentrosymmetric oxides, Chem. Mater. 10 (10) (1998) 2753–2769.
[2] K. Feng, X.X. Jiang, L. Kang, W.L. Yin, W.Y. Hao, Z.S. Lin, J.Y. Yao, Y.C. Wu, C.T. Chen, Ba6Sn6Se1: a new mixed valence selenostannate with NLO property, Dalton Trans. 42 (37) (2013) 13635–13641.
[3] K.M. Ok, E.O. Chi, P.S. Halasyamani, Bulk characterization methods for non-centrosymmetric materials: second-harmonic generation, piezoelectricity, pyroelectricity, and ferroelectricity, Chem. Soc. Rev. 35 (8) (2006) 710–717.
[4] Y. Wang, S.L. Pan, H. Yu, X. Su, M. Zhang, F.F. Zhang, J. Han, Cs4Mo5P2O22: a first strandberg-type POM with 1D straight chains of polymerized [Mo5P2O23]6- units and moderate second harmonic generation response, Chem. Commun. 49 (3) (2013) 306–308.
[5] P.S. Halasyamani, W. Zhang, Inorganic materials for UV and deep-UV nonlinear-optical applications, Inorg. Chem. 56 (20) (2017) 12077–12085.
[6] M.L. Liang, C.L. Hu, F. Kong, J.G. Mao, BiFSeO3: an excellent SHG material designed by aliovalent substitution, J. Am. Chem. Soc. 138 (30) (2016) 9433–9436.
[7] C.T. Chen, Y.C. Wu, A.D. Jiang, B.C. Wu, G.M. You, R.K. Li, S.J. Lin, New nonlinear-optical crystal: LiB_3O_5, J. Opt. Soc. Am. B 6 (4) (1989) 616–621.
[8] C.T. Chen, B.C. Wu, A.D. Jiang, G. You, A new type of ultra-violet SHG crystal, BaB_2O_4, Sci. Sin. Ser. B 28 (4) (1985) 235–243.
[9] B.C. Wu, D.Y. Tang, N. Ye, C.T. Chen, Linear and nonlinear optical properties of the $KBe_2BO_3F_2$ (KBBF) crystal, Opt. Mater. 5 (1–2) (1996) 105–109.
[10] R. Appel, C.D. Dyer, J.N. Lockwood, Design of a broadband UV-visible α-barium borate polarizer, Appl. Opt. 41 (13) (2002) 2470–2480.
[11] X.L. Chen, B.B. Zhang, F.F. Zhang, Y. Wang, M. Zhang, Z.H. Yang, S.L. Pan, Designing an excellent deep-ultraviolet birefringent material for light polarization, J. Am. Chem. Soc. 140 (47) (2018) 16311–16319.
[12] S.G. Zhao, P.F. Gong, S.Y. Luo, S.J. Liu, L.N. Li, M.A. Asghar, J.H. Luo, Beryllium-free $Rb_3Al_3B_3O_{10}F$ with reinforced interlayer bonding as a deep-ultraviolet nonlinear optical crystal, J. Am. Chem. Soc. 137 (6) (2015) 2207–2210.
[13] H.W. Yu, H.P. Wu, S.L. Pan, Z.H. Yang, X.L. Hou, X. Su, J.M. Rondinelli, $Cs_3Zn_6B_9O_{21}$: a chemically benign member of the KBBF family exhibiting the largest second harmonic generation response, J. Am. Chem. Soc. 136 (4) (2014) 1264–1267.
[14] Y.G. Shen, S.G. Zhao, Y. Yang, L.L. Cao, Z.J. Wang, B.Q. Zhao, J.H. Luo, A new KBBF-family nonlinear optical material with strong interlayer bonding, Cryst. Growth Des. 17 (8) (2017) 4422–4427.
[15] K.M. Ok, Toward the rational design of novel noncentrosymmetric materials: factors influencing the framework structures, Acc. Chem. Res. 49 (12) (2016) 2774–2785.
[16] X.H. Dong, L. Huang, C.F. Hu, H.M. Zeng, Z.E. Lin, X. Wang, K.M. Ok, G.H. Zou, $CsSbF_2SO_4$: an excellent ultraviolet nonlinear optical sulfate with a $KTiOPO_4$ (KTP)-type structure, Angew. Chem. Int. Ed. 58 (20) (2019) 6528–6534.
[17] E.J. Cho, S.J. Oh, H. Jo, J. Lee, T.S. You, K.M. Ok, Layered bismuth oxyfluoride nitrates revealing large second-harmonic generation and photocatalytic properties, Inorg. Chem. 58 (3) (2019) 2183–2190.
[18] H.P. Wu, H.W. Yu, Z.H. Yang, X.L. Hou, X. Su, S.L. Pan, K.R. Poeppelmeier, J.M. Rondinelli, Designing a deep-ultraviolet nonlinear optical material with a large second harmonic generation response, J. Am. Chem. Soc. 135 (11) (2013) 4215–4218.
[19] W.G. Zhang, H.W. Yu, H.P. Wu, P.S. Halasyamani, Phase-matching in nonlinear optical compounds: a materials perspective, Chem. Mater. 29 (7) (2017) 2655–2668.
[20] Y. Wang, B.B. Zhang, Z.H. Yang, S.L. Pan, Cation-tuned synthesis of fluorooxoborates: towards optimal deep-ultraviolet nonlinear optical materials, Angew. Chem. Int. Ed. 57 (8) (2018) 2150–2154.
[21] X.F. Wang, Y. Wang, B.B. Zhang, F.F. Zhang, Z.H. Yang, S.L. Pan, CsB_4O_6F: a congruent-melting deep-ultraviolet nonlinear optical material by combining superior functional units, Angew. Chem. Int. Ed. 56 (45) (2017) 14119–14123.
[22] B.B. Zhang, G.Q. Shi, Z.H. Yang, F.F. Zhang, S.L. Pan, Fluorooxoborates: beryllium-free deep-ultraviolet nonlinear optical materials without layered growth, Angew. Chem. Int. Ed. 56 (14) (2017) 3916–3919.
[23] Z.Z. Zhang, Y. Wang, B.B. Zhang, Z.H. Yang, S.L. Pan, Polar fluorooxoborate, NaB_4O_6F: a promising material for ionic conduction and nonlinear optics, Angew. Chem. Int. Ed. 57 (22) (2018) 6577–6581.
[24] G.Q. Shi, Y. Wang, F.F. Zhang, B.B. Zhang, Z.H. Yang, X.L. Hou, S.L. Pan, Finding the next deep-ultraviolet nonlinear optical material: $NH_4B_4O_6F$, J. Am. Chem. Soc. 139 (31) (2017) 10645–10648.
[25] M.D. Mutailipu, M. Zhang, B.B. Zhang, L. Wang, Z.H. Yang, X. Zhou, S.L. Pan, $SrB_5O_7F_3$ functionalized with $[B_5O_9F_3]^{6-}$ chromophores: accelerating the rational design of deep-ultraviolet nonlinear optical materials, Angew. Chem. Int. Ed. 57 (21) (2018) 6095–6099.
[26] Y.G. Shen, Y. Yang, S.G. Zhao, B.Q. Zhao, Z.S. Lin, C.M. Ji, L.N. Li, P. Fu, M.C. Hong, J.H. Luo, Deep-ultraviolet transparent Cs_2LiPO_4 exhibits an unprecedented second harmonic generation, Chem. Mater. 28 (19) (2016) 7110–7116.
[27] L. Li, Y. Wang, B.H. Lei, S.J. Han, Z.H. Yang, K.R. Poeppelmeier, S.L. Pan, A new deep-ultraviolet transparent orthophosphate $LiCs_2PO_4$ with large second harmonic generation response, J. Am. Chem. Soc. 138 (29) (2016) 9101–9104.
[28] W.Q. Chen, Q. Jing, W.Y. Zhang, M.H. Lee, X.F. Lu, P. Wei, Chen ZH (2019) A new cadmium-based $Pb_2Cd_3(PO_4)_2(P_2O_7)$ with two types of isolated P-O groups, Eur. J. Inorg. Chem. 9 (2019) 1273–1278.
[29] Y. Fang, Z.H. Chen, Y.J. Shi, W.Y. Zhang, X.Y. Dong, $Li_{1.5}2N_{a4.4}8C_d8(P_O4)2(_P2_O7)4$: A new mixed-anion diphosphate containing four types of dimensions groups, Inorg. Chem. Commun. 86 (7) (2017) 253–257.
[30] Z.H. Chen, Y. Fang, W.Y. Zhang, W.Q. Chen, X.F. Lu, Q. Jing, M.H. Lee, $ALiZnP_2O_7$ (A= Rb, Cs): two mixed alkali zinc pyrophosphates featuring a $[Li_2Zn_2P_4O_{20}]^{14}$ anionic skeleton, Inorg. Chem. 57 (17) (2018) 10568–10575.
[31] X.F. Lu, R.L. Wu, Q. Jing, W.Q. Chen, Y.J. Shi, X.Y. Dong, Z.H. Chen, Non-centrosymmetric $BaNaP_3O_9$ with a short deep-ultraviolet cutoff edge, J. Alloy Compd. 764 (2018) 170–176.
[32] R.E. Sykora, K.M. Ok, P.S. Halasyamani, T.E. Albrecht-Schmitt, Structural modulation of molybdenyl iodate architectures by alkali metal cations in $AMoO_3(IO_3)$ (A= K, Rb, Cs): a facile route to new polar materials with large SHG responses, J. Am. Chem. Soc. 124 (9) (2002) 1951–1957.
[33] P.S. Halasyamani, Asymmetric cation coordination in oxide materials: influence of lone-pair cations on the intra-octahedral distortion in d^0 transition metals, Chem. Mater. 16 (19) (2004) 3586–3592.
[34] Y.H. Li, H.P. Wu, B.B. Zhang, Z.H. Yang, G.P. Han, S.L. Pan, Mo^{6+} Cation enrichment of the structure chemistry of iodates: syntheses, structures, and calculations of $Ba(MoO_2)_2(IO_3)_4O$, $Ba_3[(MoO_2)_2(IO_3)_4O(OH)_4]\cdot 2H_2O$, and Sr $[(MoO_2)_6(IO_4)_2O_4]\cdot H_2O$, Inorg. Chem. 57 (15) (2018) 9376–9384.
[35] Y. Wang, S.L. Pan, X. Su, Z.H. Yang, L.Y. Dong, M. Zhang, New molybdenum(VI) phosphates: synthesis, characterization, and calculations of centrosymmetric $RbMoO_2PO_4$ and noncentrosymmetric $Rb_4Mo_5P_2O_{22}$, Inorg. Chem. 52 (3) (2013) 1488–1495.
[36] P.C. Du, A. Dolbecq, P. Mialane, J. Marrot, F. Sécheresse, Template synthesis of $\{(MoV_2O_4)(O_3PCH_2PO_3)\}_n$ clusters (n = 3, 4, 10): solid state and solution studies, Dalton Trans. 8 (2004) 1259–1263.
[37] J.H.E. King, L.A. Mundi, K.G. Strohmaier, R.C. Haushalter, A synchrotron single crystal x-ray structure determination of a small crystal: Mo-Mo double bonds in the 3-D microporous molybdenum phosphate $NH_4[Mo_2P_2O_{10}]\cdot H_2O$, J. Solid State Chem. 92 (1) (1991) 1–7.
[38] J.C.A. Boeyens, G.J. Mcdougal, J.V.R. Smit, Crystallographic study of the ammonium/potassium 12-molybdophosphate ion-exchange system, J. Solid State Chem. 18 (2) (1976) 191–199.
[39] J.H.E. King, L.A. Mundi, K.G. Strohmaier, R.C. Haushalter, A synchroton single crystal x-ray structure determination of $(NH_4)_3Mo_4P_3O_{16}$: a microporous molybdenum phosphate with $Mo_4O_4^{6+}$ cubes, J. Solid State Chem. 92 (1) (1991) 154–158.
[40] Y. Xu, J.Q. Xu, G.Y. Yang, G.D. Yang, Y. Xing, Y.H. Lin, H.Q. Jia, $(NH_4)_3[PMo_{12}O_{40}]\cdot 21H_2O$, Acta Cryst. 54 (1) (1998) 9–11.
[41] S.E. Lister, V.J. Rixom, J.S. Evans, Structural and mechanistic studies of the dehydration of $MoO_2PO_3OH\cdot 3H_2O$ and the In situ identification of two new molybdenum phosphates, Chem. Mater. 22 (18) (2010) 5279–5289.
[42] A. Müller, S. Sarkar, S.Q.N. Shah, H. Bögge, M. Schmidtmann, S. Sarkar, V. Schünemann, Archimedean synthesis and magic numbers: "sizing" giant molybdenum-oxide-based molecular spheres of the keplerate type, Angew. Chem. Int. Ed. 38 (21) (1999) 3238–3241.
[43] A. Müller, S.K. Das, S. Talismanov, S. Roy, E. Beckmann, H. Bögge, Y. Zhou, Trapping cations in specific positions in tuneable "artificial cell" channels: new nanochemistry perspectives, Angew. Chem. Int. Ed. 42 (41) (2003) 5039–5044.
[44] F.Y. Li, L. Xu, Coordination assemblies of polyoxomolybdate cluster framework: from labile building blocks to stable functional materials, Dalton Trans. 40 (16) (2011) 4024–4034.
[45] R. Essehli, B. El Bali, S. Benmokhtar, H. Fuess, I. Svoboda, S. Obbade, Synthesis, crystal structure and infrared spectroscopy of a new non-centrosymmetric mixed-anion phosphate $Na_4Mg_3(PO_4)_2(P_2O_7)$, J. Alloy. Compd. 493 (1–2) (2010) 654–660.
[46] E. Kotsapa, M.T. Weller, $[NH_4]_{12}[(MoO_2)_2O(HPO_4)_2]_4[PO_4]X$, X = Cl, Br—new porous layer molybdenophosphates with embedded multiple anionic and cationic guests, Dalton Trans. 3 (2009) 418–420.
[47] SAINT-Plus, V. (2000) 6.02A, Bruker analytical X-ray instruments, Inc. Madison, WI.
[48] G.M. Sheldrick, Crystal structure refinement with SHELXL, Acta Cryst 71 (1) (2015) 3–8.
[49] A.L.J. Spek, Single-crystal structure validation with the program PLATON, J. Appl. Crystallogr. 36 (1) (2003) 7–13.
[50] P. Kubelka, F. Munk, An article on optics of paint layers, Z. Tech. Phys. 12 (1931) 593–601.
[51] J. Tauc, Absorption edge and internal electric fields in amorphous semiconductors, Mater. Res. Bull. 5 (8) (1970) 721–729.
[52] S.K. Kurtz, T.T. Perry, A powder technique for the evaluation of nonlinear optical materials, J. Appl. Phys. 39 (8) (1968) 3798–3813.
[53] J.P. Dougherty, S.K. Kurtz, A second harmonic analyzer for the detection of non-centrosymmetry, Appl. Crystallogr. 9 (2) (1976) 145–158.
[54] L.C. Tang, J.Y. Huang, C.S. Chang, M.H. Lee, L.Q. Liu, New infrared nonlinear optical crystal CsGeBr 3: synthesis, structure and powder second-harmonic generation properties, J Phys. Condens. Mater. 17 (46) (2005) 7275–7286.
[55] J.P. Perdew, M. Levy, Physical content of the exact Kohn-Sham orbital energies: band gaps and derivative discontinuities, Phys. Rev. Lett. 51 (20) (1983) 1884–1887.
[56] A.M. Rappe, K.M. Rabe, E. Kaxiras, J.D. Joannopoulos, Optimized pseudopotentials, Phys. Rev. B 41 (2) (1990) 1227–1230.
[57] R.F. Bader, Vibrationally induced perturbations in molecular electron distributions,

Can. J. Chem. 40 (6) (1962) 1164–1175.
[58] B.H. Lei, Z.H. Yang, S.L. Pan, Enhancing optical anisotropy of crystals by optimizing bonding electron distribution in anionic groups, Chem. Commun. 53 (19) (2017) 2818–2821.
[59] X.Y. Dong, Q. Jing, Y.J. Shi, Z.H. Yang, S.L. Pan, K.R. Poeppelmeier, J.M. Rondinelli, $Pb_2Ba_3(BO_3)_3Cl$: A material with large SHG enhancement activated by Pb-chelated BO_3 groups, J. Am. Chem. Soc. 137 (29) (2015) 9417–9422.
[60] Q. Jing, Z.H. Yang, S.L. Pan, D.F. Xue, Contribution of lone-pairs to birefringence affected by the Pb(II) coordination environment: a DFT investigation, PCCP 17 (34) (2015) 21968–21973.